Microstructures and Mechanical Properties of Ti3SiC2/Al2O3 and Ti3SiC2-TiC/Al2O3 Composite Ceramics by Modifying Al2O3 Content Via in-situ Synthesized

Jun Ji
University of Jinan
Xuye Wang
University of Jinan
Jinman Yu
University of Jinan
Qinggang Li
University of Jinan
Zhi Wang (wangzhi@ujn.edu.cn)
University of Jinan https://orcid.org/0000-0002-8001-6648
Guopu Shi
University of Jinan

Research Article

Keywords: Ti3SiC2/Al2O3 composite ceramics, Ti3SiC2-TiC/Al2O3 composite ceramics, in-situ synthesis, mechanical properties

Posted Date: August 26th, 2020

DOI: https://doi.org/10.21203/rs.3.rs-64823/v1

Microstructures and mechanical properties of Ti_3SiC_2/Al_2O_3 and Ti_3SiC_2-TiC/Al_2O_3 composite ceramics by modifying Al_2O_3 content via in-situ synthesized

Jun Ji, Xuye Wang, Jinman Yu, Qinggang Li, Zhi Wang*,Guopu Shi**,

School of Material Science and Engineering, University of Jinan, Jinan 250022, China

* *First corresponding author: wangzhi@ujn.edu.cn;*

** *Second corresponding author: ss_shigp@ujn.edu.cn;*

Abstract

Ti_3SiC_2/Al_2O_3 and Ti_3SiC_2-TiC/Al_2O_3 composite ceramics with various Al_2O_3 fractions were prepared by Ti, Si, Al, TiC and Al_2O_3 powers via in-situ reaction. Al_2O_3 contents in raw materials could influence the reaction process of Ti_3SiC_2 generated. It would lead to react completely when the Al_2O_3 volume percentage between 50% to 70%, otherwise TiC as an impurity would be found. Finally the Ti_3SiC_2/Al_2O_3 composites with 54.4 wt% Ti_3SiC_2, and Ti_3SiC_2-TiC/Al_2O_3 composites with 54.7 wt% Ti_3SiC_2 and 9.2 wt% TiC were fabricated successfully. There were two types of TiC existed in composites, called intragranular and intergranular particles. The Ti_3SiC_2-TiC/Al_2O_3 composite ceramics with 9.2 wt% TiC showed the higher mechanical properties than Ti_3SiC_2/Al_2O_3 composite. From the analyzing of microcrack propagation paths, the dispersed TiC particles as reinforcement agents would cause significant crack deflection, improving the flexural strength and fracture toughness up to 492 MPa and 7.8 MPa.$m^{1/2}$ respectively.

Keywords: *Ti_3SiC_2/Al_2O_3 composite ceramics; Ti_3SiC_2-TiC/Al_2O_3 composite ceramics; in-situ synthesis; mechanical properties.*

1.Introduction

Ternary MAX phase ceramics, where M is an early transition metal, A is an A group element and X is carbon or nitrogen, have captured considerable attentions for their combination of metallic and ceramic

properties, making them possible candidates used as structural materials at high temperatures and/ or in corrosive environments[1-3]. Ti_3SiC_2 is the most extensively studied MAX phase, has been synthesized by various pressure sintering methods at high temperatures, which can be mainly conducted by the following three reactions[4-6]:

$$3Ti + Si + 2C \rightarrow Ti_3SiC_2 \cdots\cdots (1)$$
$$3Ti + SiC + C \rightarrow Ti_3SiC_2 \cdots\cdots (2)$$
$$Ti + Si + 2TiC \rightarrow Ti_3SiC_2 \cdots\cdots (3)$$

However, it is not facile to fabricate the single-phase Ti_3SiC_2 due to its narrow phase region as well as impurity of TiC would be generated inevitably[7,8]. In order to address this problem, Al is often used in in-situ synthesis of Ti_3SiC_2 as sintering additive[9-12]. Molten Al could remove oxygen, fill gaps and provide a bridging effect among the reacting powder particles, all of which could promote the diffusion reaction[13]. As a result, TiC as impurity will decrease obviously when suitable contents of Al are introduced into in-suit synthesis[13-15].

Although Ti_3SiC_2 has to be seen as a potential structure/functional material as its combined metallic- and ceramic-like properties, the relatively low strength and hardness limit its further application. Al_2O_3 ceramics with superb performances such as low price, high hardness, good corrosion resistance and stability at elevated temperatures[16], has been incorporated into Ti_3SiC_2 to improve the mechanical properties. Composite ceramics can be synthesized by various of sintering methods,

such as self-propagating high-temperature sintering (SHS)[17], spark plasma sintering (SPS)[18] and hot pressing (HP)[19,20]. Qi et al.[21] fabricated Ti_3SiC_2/Al_2O_3 composites with various volume contents of Ti_3SiC_2 under different sintering processes using Ti_3SiC_2 and Al_2O_3 as raw materials. Cai et al.[22] reported the $Ti_3SiC_2/TiC\text{-}Al_2O_3$ composites synthesized by reactive hot pressing, suggesting that the composites with 20 wt% additions showed the highest flexural strength of 649 MPa and 10 wt% additions displayed the best fracture toughness of 7.15 $Mpa^{1/2}$. Pourali et al.[23] prepared high-purity Ti_3SiC_2 and Ti_3SiC_2/Al_2O_3-Ni composites with different Al_2O_3-Ni contents. The composites exhibited lower flexural strength and higher compressive strength than single-phase Ti_3SiC_2.

In our previous work[19], $Ti_3SiC_2/TiC\text{-}Al_2O_3$ composites were synthesized from Al_2O_3, Ti and SiC powders, while amounts of TiC as third-phase existed in composite ceramics. Now we prepared biphase Ti_3SiC_2/Al_2O_3 and multiphase $Ti_3SiC_2\text{-}TiC/Al_2O_3$ composites using Ti, Si, Al, TiC and Al_2O_3 powders via hot pressing. It can influence the generated reaction of Ti_3SiC_2 by modifying the contents of Al_2O_3, and the TiC disappear with the volume percentage of Al_2O_3 from 50 to 70%. Although our work is fundamental, it is rare to see the high-purity Ti_3SiC_2/Al_2O_3 composites with 50 vol% Ti_3SiC_2 through in-situ synthesis. The composition, micro-structure and mechanical properties of all

samples were further investigated.

2. Materials and experimental methods

The raw materials employed herein were fine powders of the following types: dry Al_2O_3 (99.6% pure, ~0.5 μm), Ti (99.6% pure, ~5 μm), TiC (99.5% pure, ~2 μm), Si (99% pure, ~1 μm), and Al (99% pure, ~30 nm). The proportions of each group with different volume fractions of Al_2O_3 and mixed powders are shown in Tab. 1.

The mixed powders in the molar ratio of 1.0Ti/2.0TiC/1.2Si/0.3Al and Al_2O_3 powders were dispersed evenly in ethanol at 200 rpm for 4 h in a planetary mill (XQM-2, China), following which the resulting slurry was dried in a drying oven at 70 °C and sifted using a 50 mesh sifter. Subsequently, the raw materials were sintered in a vacuum hot-pressing furnace (VVPgr-80–2300, China) at 1450 ℃ for 1.5 h under a vacuum pressure of $<8.0\times10^{-3}$ MPa, and the pressure was maintained at 30 MPa below uniaxial pressure when the sintering temperature was 1450 ℃. Finally, the sintered samples were allowed to cool naturally to room temperature prior to their removal from the furnace.

The obtained samples were polished using SiC powder and then cut into long columns measuring 3 mm × 4 mm × 3 mm using an inner circle cutting machine with a chamfering and span of 0.3 and 30 mm, respectively. All samples were then cleaned under ultrasonication in ethanol over 20 min. The density of samples were determined by using

the Archimedes water immersion method. The flexural strength and fracture toughness of the samples were measured using the three-point bending method on an electromechanical universal testing machine (CMT5504, MTSSYSTEMS, China) with a cross-head speed of 0.5 mm/min and a span of 30 mm. The microhardness of the samples was determined using a Vickers hardness tester (HV-100IS, China) at a load of 100 N for 20 S. The phase compositions of the obtained samples were determined by XRD (D8 ADVANCE, Bruker). Microstructural investigations were performed by SEM (FEIQUANTA FEG 250, USA) and TEM (Tecnai G2F20).

Table 1. Compositions of raw materials.

Sample	Al_2O_3 (vol%)	Mixed Power (vol%)
1	80	20
2	70	30
3	60	40
4	50	50
5	40	60

3. Results and discussion

3.1 Composition and microstructure

XRD patterns of the synthesized composites ceramics are shown in Fig 1. Sample 1 was composed of Ti_3SiC_2, Al_2O_3 and TiC phase, and the

relatively lower peak of TiC indicated the less impurity content as well. As the volume fractions of Al_2O_3 decreased from 70% to 50%, the intensity of the TiC peak vanished. Samples 2-4 consisted only of the Al_2O_3 and Ti_3SiC_2 phases, indicating that the mixed powder reacted completely during the sintering process. However, as displayed in sample 5, when the volume percentage of Al_2O_3 down to 40%, amounts of TiC were detected again.

The mass fraction of each phase was calculated by the following equation:

$$W_i = \frac{I_i / K_i}{\sum_{i=1}^{n} I_i / K_i} \times 100\% \qquad (1)$$

Where W_i was the mass fraction of i phase, I_i was the intensity of selected lines in the diffraction pattern of i phase, K_i was the reference intensity of i phase based on RIR value. In this method, the mass fraction was calculated according to the intensity of the sharp peaks for each phase. Thus, (104), (104) and (200) diffraction peaks were selected for analysis of Ti_3SiC_2, Al_2O_3 and TiC phase, respectively. The mass fraction of each phase was shown in Tab. 2. Data based on quantitative method from eq. (1) indicated that the Al_2O_3 content could affect the in-situ sintering reaction of Ti_3SiC_2. Optimum Al_2O_3 content (45.6-66.4 wt%) would produce a high-purity Ti_3SiC_2 phase without any TiC impurity when sintering was carried out at 1450 °C, 30 MPa for 90 min. While the Al_2O_3 fractions beyond or below this range resulted in an incomplete in-situ

reaction, leading to the formation of the TiC phases.

Tab. 2. The mass fraction of Ti_3SiC_2, Al_2O_3 and TiC phase.

	Al_2O_3 (wt%)	Ti_3SiC_2 (wt%)	TiC (wt%)
1	76.8	19.7	3.5
2	66.4	33.6	-
3	57.9	42.1	-
4	45.6	54.4	-
5	36.1	54.7	9.2

TEM micrograph and SEAD patterns of sample 5 were presented in Fig. 2. Fig. 2a and 2b exhibited that the small-size TiC particles were distributed inside the Al_2O_3 and Ti_3SiC_2 crystal respectively, while large-size TiC particles were found around grain boundary (Fig. 3c). The size of intragranular particles are below 50nm while intergranular particles are above 200nm. This phenomenon was also reported by Chai[24] and Wang[25]. Furthermore, selected area electron diffraction (SEAD) analysis of the area indicated by the white oval is illustrated in Fig. 2d, 2e and 2f. For Ti_3SiC_2, the d-spacings of the three diffraction spots are 0.156, 0.343, and 0.141 nm respectively, which are consistent with the (1 1 0), (0 0 5), and (1 1 5) crystal planes of the Ti3SiC2 grains. The incident beam is parallel to the [1 -1 0] axis. Similarly, the (0 1 2), (1 0 1), and (1 1 3) planes of the Al_2O_3 crystal with zone axis [1 2 -1] and (1 1 1), (2 0 0) and (3 1 1) planes of TiC particle with zone axis [0 1 -1] are also indexed.

SEM back scattered electron image of synthesized composite ceramics was shown in Fig. 3. The diameters of the Ti_3SiC_2 and Al_2O_3 grains were approximately 2 – 5 μm, and no abnormal growth was observed. TiC gains were clearly observed in the fracture surface of sample 5 (Fig. 2e), while the other four groups only consist of Ti_3SiC_2 and Al_2O_3 crystals. Because sample 1 was only composed of 3.5 wt% TiC, most of which embedded in the Ti_3SiC_2 and Al_2O_3 grains, resulting in TiC particles undetected in Fig 3a. In addition, the interface combination was close and no obvious pores could be found, demonstrating the sintering densification of the Ti_3SiC_2/Al_2O_3 ceramics.

Fig. 4 shows the relative density of samples 1-5. It can be clearly found that the relative density of all the samples are more than 99%, and there is no obvious trend of patterns as the decreased of Al_2O_3, revealing sintering densification of Ti_3SiC_2/Al_2O_3 and Ti_3SiC_2-TiC/Al_2O_3 composite ceramics.

3.2 Mechanical properties

The mechanical properties including Vickers' hardness, flexural strength, and fracture toughness of samples 1–5 are described in Figure 5. With the reducing of Al_2O_3, the Vickers' hardness of the samples1-4 decline simultaneously (Fig. 5a). Sample 4 shows the lowest Vickers' hardness (14.6 GPa) among all the samples investigated possibly due to

the mass of Ti_3SiC_2, while sample 5 displays higher hardness compared to 4 on account of TiC generated. Fig. 5b shows the flexural strength of samples 1–5. As can be seen from the figure, the flexural strength of the composites first decrease and then increase a bit. Compared to sample 4, the strength of sample 5 improves from 485 to 492 MPa. The curve of toughness displays uptrend from 5.4 to 7.8 $MPa.m^{1/2}$ with the increasing of in-situ generated Ti_3SiC_2 content. Sample 5 owns the higher fracture toughness than sample 4 mainly because of the TiC particles, considering approximate fractions of Ti_3SiC_2 in both specimen.

3.3 Microcrack analysis

Samples 4 and 5 were selected for microcrack analysis because of the superior toughness. As can be found in Fig. 6, both samples showed irregular fracture paths, clearly indicating that they fractured in both intergranular and transgranular modes. It should be pointed out that transgranular fracture and particle pullout were mainly observed in laminar Ti_3SiC_2 grains, which absorbed most of the crack propagation energy and caused significant deflection and increase in the crack propagation path. In addition, there is a pit of square particle with the diameter of 200nm in Fig. 6c, which most likely result from the pullout of TiC nano-particle. TiC grains with such small size preferred being pulled out rather than cleaved. Moreover, TiC as intergranular particle would result in crack deflection. When a crack met with the TiC particle, the

crack direction changed due to the hindering effect of TiC. The deflection would increase the demand of fracture energy, which is beneficial to improve the fracture toughness of composite ceramics.

Al_2O_3 ceramics have high strength and low fracture toughness, and the fracture mode is mainly intergranular fracture. As shown in Fig.7, in the Al_2O_3 ceramics, the microcracks propagated along the vulnerable grain boundaries, resulting in the formation of macroscopic cracks and making the ceramics fragile. Ti_3SiC_2 with low strength and high toughness, as the increasing of its fractions, the composite ceramics caused transgranular fracture and particle pullout, resulting in the absorption of a large amount of fracture energy, which contribute to the improvement in toughness. When part of Al_2O_3 was replaced by TiC, the fine intergranular particle would provide dispersion strengthening and toughening effect. Thus the Ti_3SiC_2-TiC/Al_2O_3 composite ceramics displays higher flexural strength and fracture toughness than Ti_3SiC_2/Al_2O_3, based on the same Ti_3SiC_2 fractions as a prerequisite.

4. Conclusion

In this research, Ti_3SiC_2/Al_2O_3 and Ti_3SiC_2-TiC/Al_2O_3 composite ceramics with different Al_2O_3 contents were synthesized by in-situ reaction via hot pressing sintering. Based on the analysis above, the conclusions of this paper can be summarized as follows:

(1) The volume fractions of Al_2O_3 in raw materials could affect the

reaction process of in-situ synthesis of Ti_3SiC_2 . When the Al_2O_3 volume percentage between 50% to 70%, the reaction will finish completely, otherwise TiC as an impurity would be found.

(2) Based on the quantitative method, the maximum of Ti_3SiC_2 mass fractions is 54.4% in Ti_3SiC_2/Al_2O_3 composites. To the best of our knowledge, this is the first report on Ti_3SiC_2/Al_2O_3 composites with high contents of Ti_3SiC_2 by in-situ reaction.

(3) Under the premise of equal Ti_3SiC_2 contents, Ti_3SiC_2-TiC/Al_2O_3 composite ceramics show better mechanical properties than Ti_3SiC_2/Al_2O_3 due to the dispersed TiC as the reinforcement agent.

Acknowledgements

The authors appreciate the financial support of the National Natural Science Foundation of China under Grant No. 51872118 and the Natural Science Foundation of Shandong Province under Grant No. ZR2019MEM055.

Conflicts of Interest

We declare that we have no financial and personal relationships with other people or organizations that can inappropriately influence our work, and we do not have any commercial or associative interest that represents a conflict of interest in connection with the work submitted.

References

[1] Xie J, Wang XH, Li AJ, Li FZ, Zhou YC. Corrosion behavior of selected $M_{n+1}AXn$ phases in hot concentrated HCl solution: Effect of a element and MX layer. *Corros Sci* 2012, **60:** 129–135.

[2] Zhou YC and Sun ZM. Temperature fluctuation/hot pressing synthesis of Ti_3SiC_2. *J Mater Sci* 2000, **35:**4343-4346.

[3] Zhang H, Li ZJ, Zhang C, Li JL, Wang XH, Zhou YC. Nb doping in Ti_3AlC_2: Effects on phase stability, high-temperature compressive properties and oxidation resistance. *J Eur Ceram Soc* 2017, **37:** 3641–3645.

[4] Li JF, Sato F, Watanabe R. Synthesis of Ti_3SiC_2 polycrystals hot-isostatic pressing of the elemental powders. *J Mater Sci Lett* 1999, **18:** 1595-1597.

[5] Barsoum MW, Raghy T, Rawn CJ, Porter WD, Wang H, Payzant EA, Hubbard CR . Thermal properties of Ti_3SiC_2. *J Phys Chem Solids* 1999, **60:** 429–439.

[6] Barsoum MW and Raghy T. Synthesis and characterization of a remarkable ceramic: Ti_3SiC_2. *J Am Ceram Soc* 1996, **79:**1953–1956.

[7] Yang S, Sun ZM, Hashimoto H, Abe T. Ti_3SiC_2 powder synthesis from Ti/Si /TiC powder mixtures. *J Alloys Comp* 2003, **358:** 168–172.

[8] Ghosh NC, Harimkar SP. Phase analysisandwearbehaviorof in-situ spark plasmasintered Ti_3SiC. *Ceram Int* 2013, **39:** 6777–6786.

[9] Li JF, Matsuki T, Watanabe R. Fabrication of highly dense Ti_3SiC_2 ceramics by pressureless sintering of mechanically alloyed elemental powders. *J Mater Sci* 2003, **38:** 2661-2666.

[10] Zou Y, Sun ZM, Tada S, Hashimoto H. Effect of Al addition on low-temperature synthesis of Ti_3SiC_2 powder. *J Alloys Comp* 2008, **461:** 579–584.

[11] Zhang HB, Zhou YC, Bao YW, Li MS. Improving the oxidation resistance of Ti_3SiC_2 by forming a $Ti_3Si_{0.9}Al_{0.1}C_2$ solid solution. *Acta Mater* 2004, **52:** 3631–3637.

[12] Zhang HB, Zhou YC, Bao YW, Li MS, Wang JY. Intermediate phases in synthesis of Ti_3SiC_2 and $Ti_3Si(Al)C_2$ solid solutions from elemental powders. *J Eur Ceram Soc* 2006, **26:** 2373–2380.

[13] Sato K, Mishra M, Hirano H, Hu C, Sakka Y. Pressureless sintering and reaction mechanisms of Ti_3SiC_2 Ceramics. *J Am Ceram Soc* 2014, **97:** 1407-1412.

[14] Pourebrahim A, Baharvandi H, Foratirad H, Ehsani N. Low temperature synthesis of high-purity Ti_3SiC_2 via additional Si through spark plasma sintering. *J Alloys Comp* 2019, **789:** 313–322.

[15] Li XH, Xu L, Chen QY, Cao XX, Liu LX, Wang Y, Zhang HB, Meng CM, et al . Investigation of formation mechanism of Ti_3SiC_2 by high pressure and high-temperature synthesis. *High Pressure Res* 2018, **38:** 440-447.

[16] Wu DJ, Lu F, Zhao DK, Ma GY, Li CJ, Ding J, Niu FY. Effect of doping SiC particles on cracks and pores of Al_2O_3 – ZrO_2 eutectic ceramics fabricated by directed laser deposition. *J Mater Sci* 2019, **54:** 9321-9330.

[17] Yeh CL, Li RF, Shen YG. Formation of Ti_3SiC_2-Al_2O_3 in situ composites by SHS involving thermite reactions. *J Alloys Comp* 2009, **478:** 699-704.

[18] Wang HJ, Jin ZH, Miyamoto Y. Ti_3SiC_2/Al_2O_3 composites prepared by SPS. *Ceram Int* 2003, **29:** 539–542.

[19] Qi FF, Wang Z, Wu JY, Xu HQ, Kou JJ, Zhang L. Improved mechanical properties of Al_2O_3 ceramic by in-suit generated Ti_3SiC_2 and TiC via hot pressing sintering. *Ceram Int* 2017, **43:** 10691–10697.

[20] Liu Y, Luo F, Su JB, Zhou WC, Zhu DM. Mechanical, dielectric, and microwave-absorption properties of alumina ceramic containing dispersed Ti_3SiC_2. *J Electron Mater* 2015, **44:** 867-873.

[21] Qi FF, Shi GP, Xu K, Su T, Wang Z, Wu JY, Li QG, Wu H,et al. Microstructure and mechanical properties of hot pressed Ti_3SiC_2/Al_2O_3. *Ceram Int* 2019, **45:** 11099–11104.

[22] Cai YZ, Yin HF, Pan LQ, Chen PJ, Sun GL. Microstructures and mechanical properties of Ti_3SiC_2/TiC-Al_2O_3 composites synthesized by reactive hot pressing. *Mater Sci Eng A* 2013, **571:** 137–143.

[23] Pourali Z, Sovizi MR, Yaftian MR, Amiri Z, Emami SM, Shahed HE. Microstructures and mechanical behavior of Ti_3SiC_2/Al_2O_3-Ni composites synthesized by pulse discharge sinterin. *J Mater Eng Perform* 2018, **27:** 3600-3609.

[24] Chai JL, Zhu YB, Wang ZG, Shen TL, Liu YW, Niu LJ, Li SF, Yao CF, et al. Microstructure and mechanical properties of SPS sintered Al_2O_3–ZrO_2(3Y)–SiC ceramic composites. *Mater Sci Eng A* 2020, **781**: DOI: 10.1016/j.msea.2020.139197

[25] Wang YJ, Yan QZ. Microstructure and strengthening mechanism of grain boundary strengthened W-ZrB_2 alloy. *J Mater Res Technol* 2020, 9: 4007-4015.

Figure Captions

Fig. 1. XRD patterns of samples sintered by hot pressing.

Fig. 2. TEM micrograph and SEAD patterns of sample 5. Intragranular TiC particles in (a) Ti_3SiC_2 and (b) Al_2O_3 crystal; Intergranular TiC around grain boundary (c); SEAD patterns of Ti_3SiC_2 (d) and Al_2O_3 (e) and TiC (f).

Fig. 3. SEM image of all samples. (a): sample 1; (b): sample 2; (c): sample 3; (d): sample 4; (e): sample 5.

Fig. 4 The relative density of samples 1-5.

Fig. 5. The mechanical properties of sample 1-5. (a) Vickers' hardness; (b) flexural strength and fracture toughness.

Fig. 6. Fracture mode for sample 4:(a) and (b); sample 5: (c) and (d).

Fig.7 The diagram of microcrack propagation paths in Al_2O_3 and Ti_3SiC_2-TiC/Al_2O_3 ceramics.

Figures

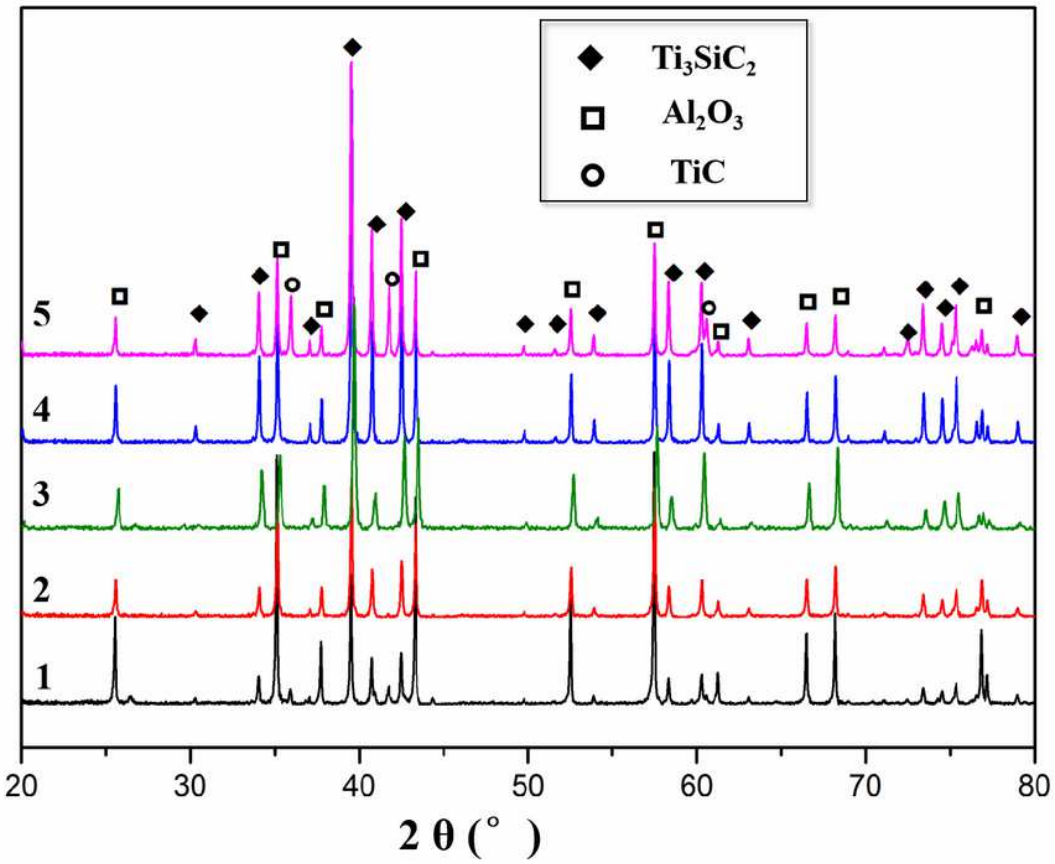

Figure 1

XRD patterns of samples sintered by hot pressing.

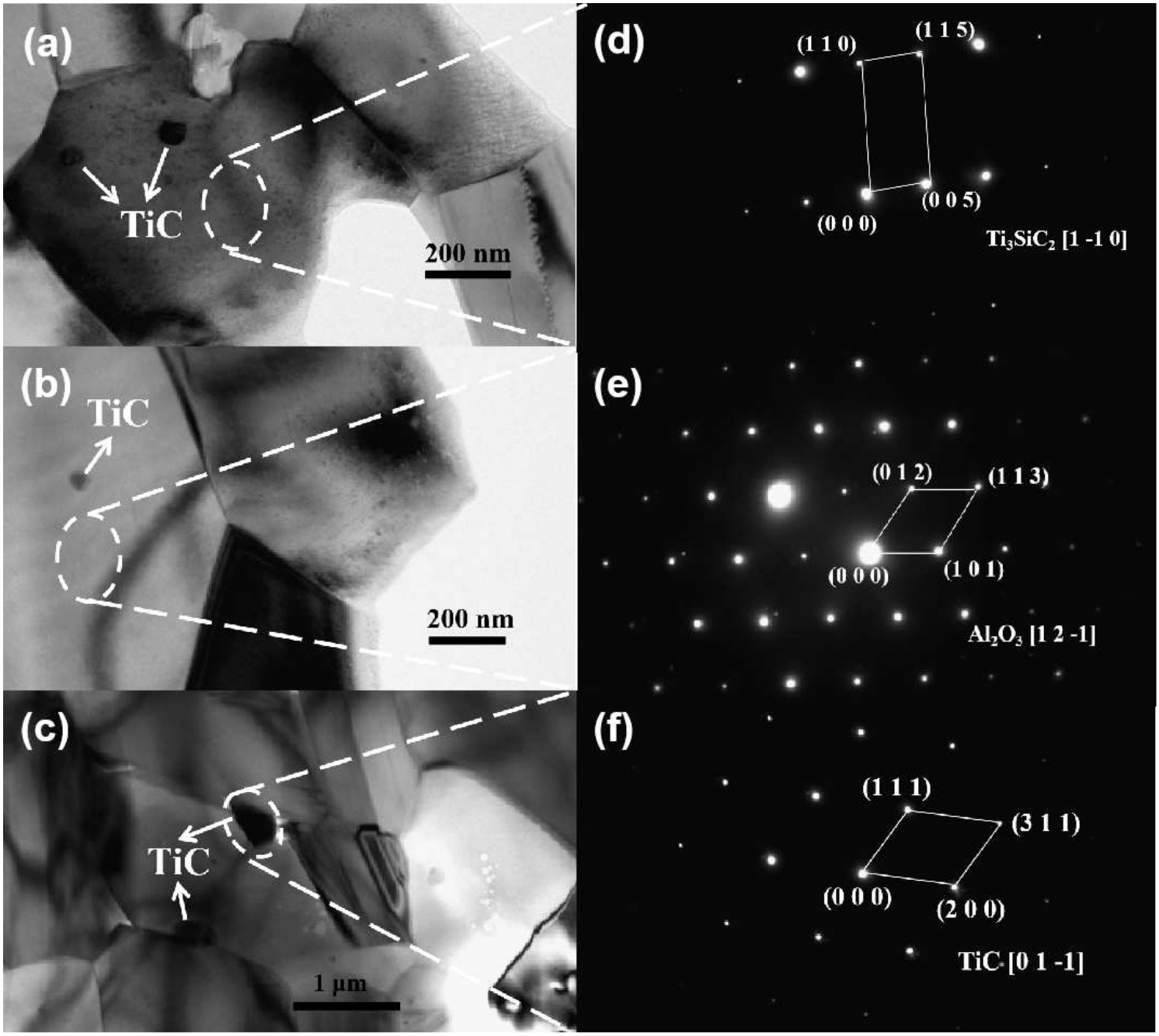

Figure 2

TEM micrograph and SEAD patterns of sample 5. Intragranular TiC particles in (a) Ti3SiC2 and (b) Al2O3 crystal; Intergranular TiC around grain boundary (c); SEAD patterns of Ti3SiC2 (d) and Al2O3 (e) and TiC (f).

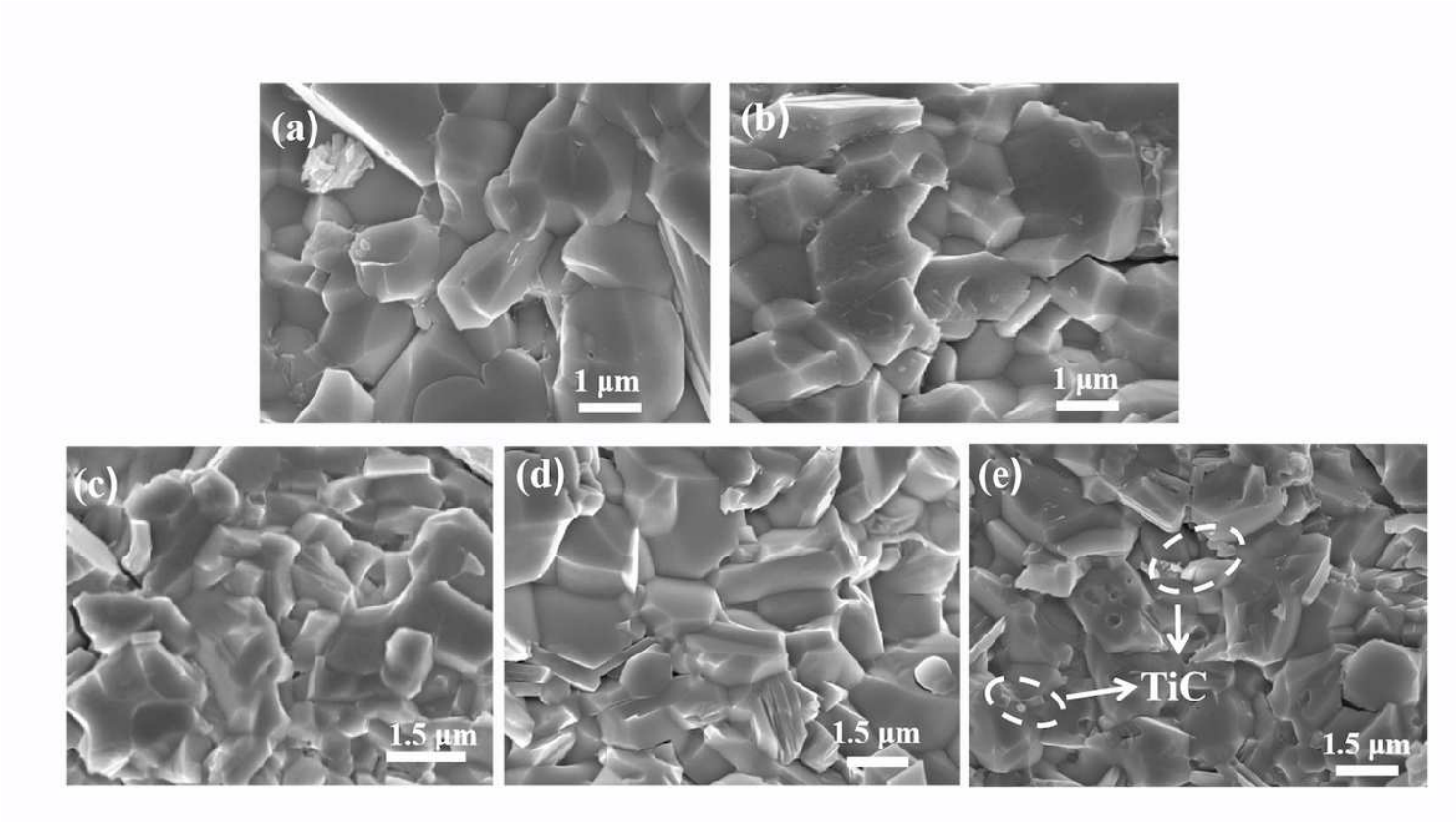

Figure 3

SEM image of all samples. (a): sample 1; (b): sample 2; (c): sample 3; (d): sample 4; (e): sample 5.

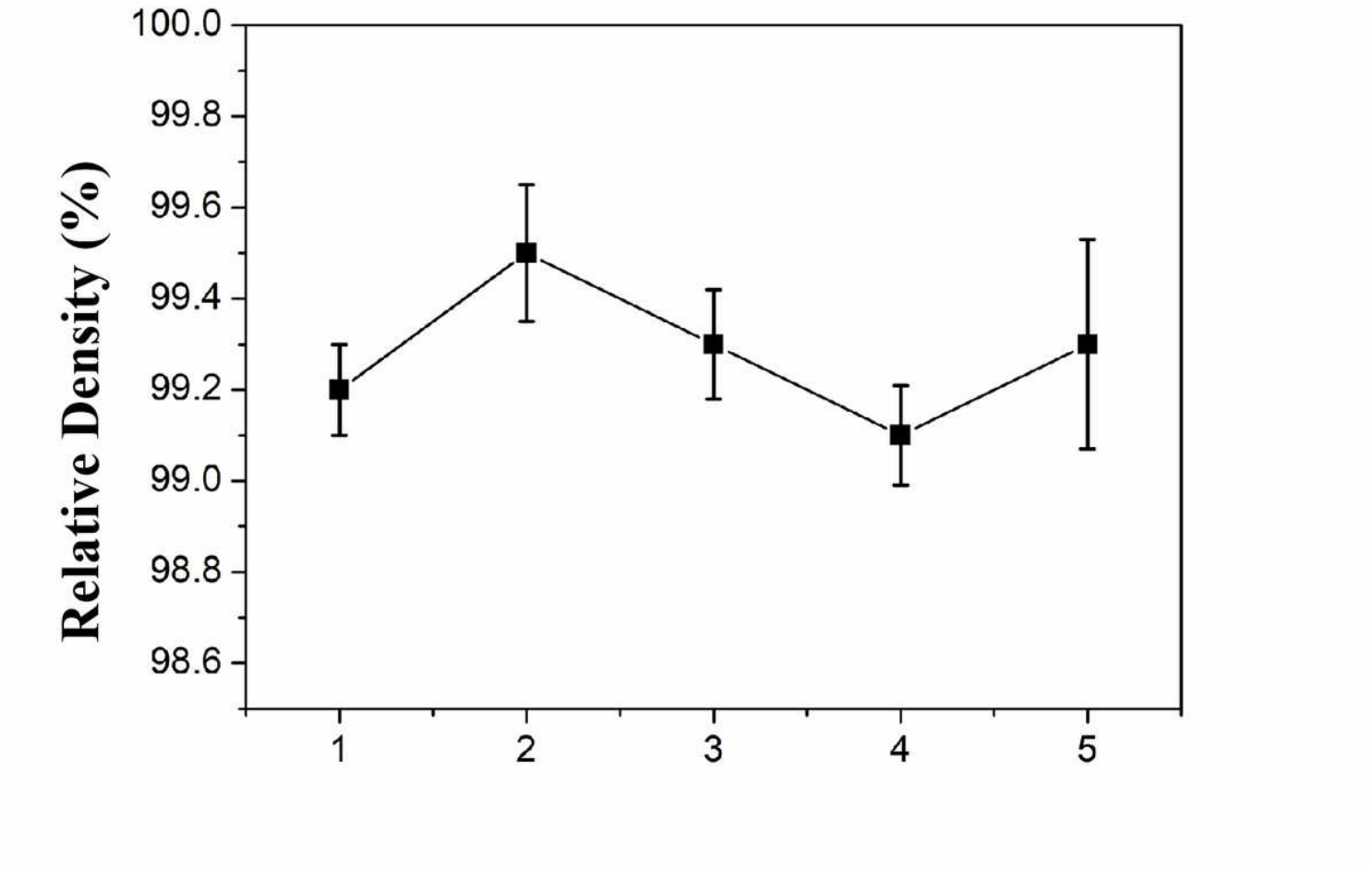

Figure 4

The relative density of samples 1-5.

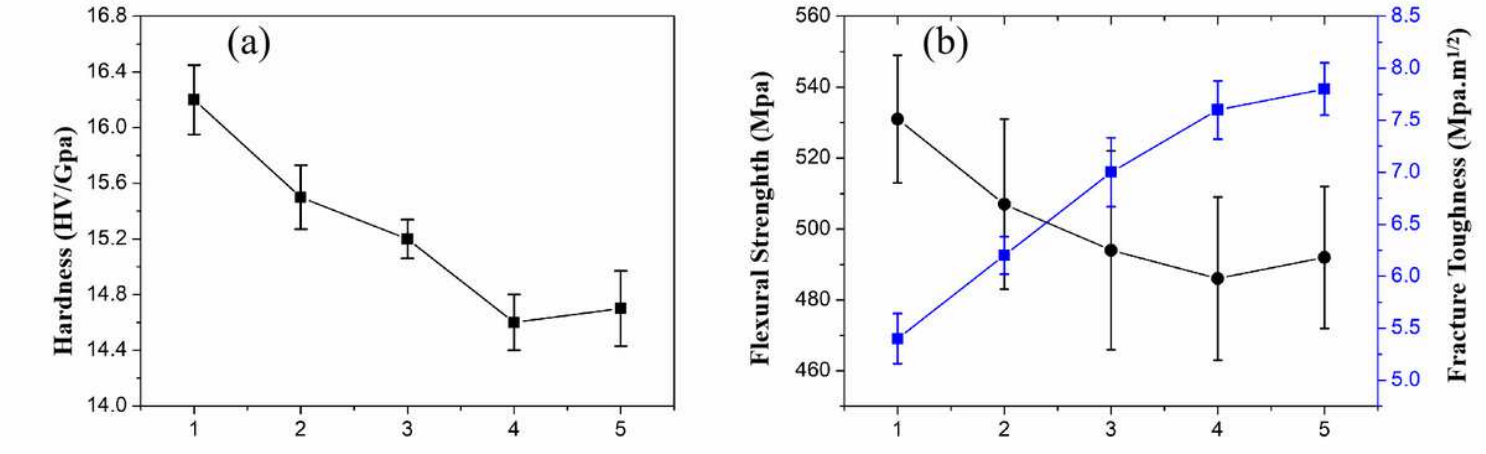

Figure 5

The mechanical properties of sample 1-5. (a) Vickers' hardness; (b) flexural strength and fracture toughness.

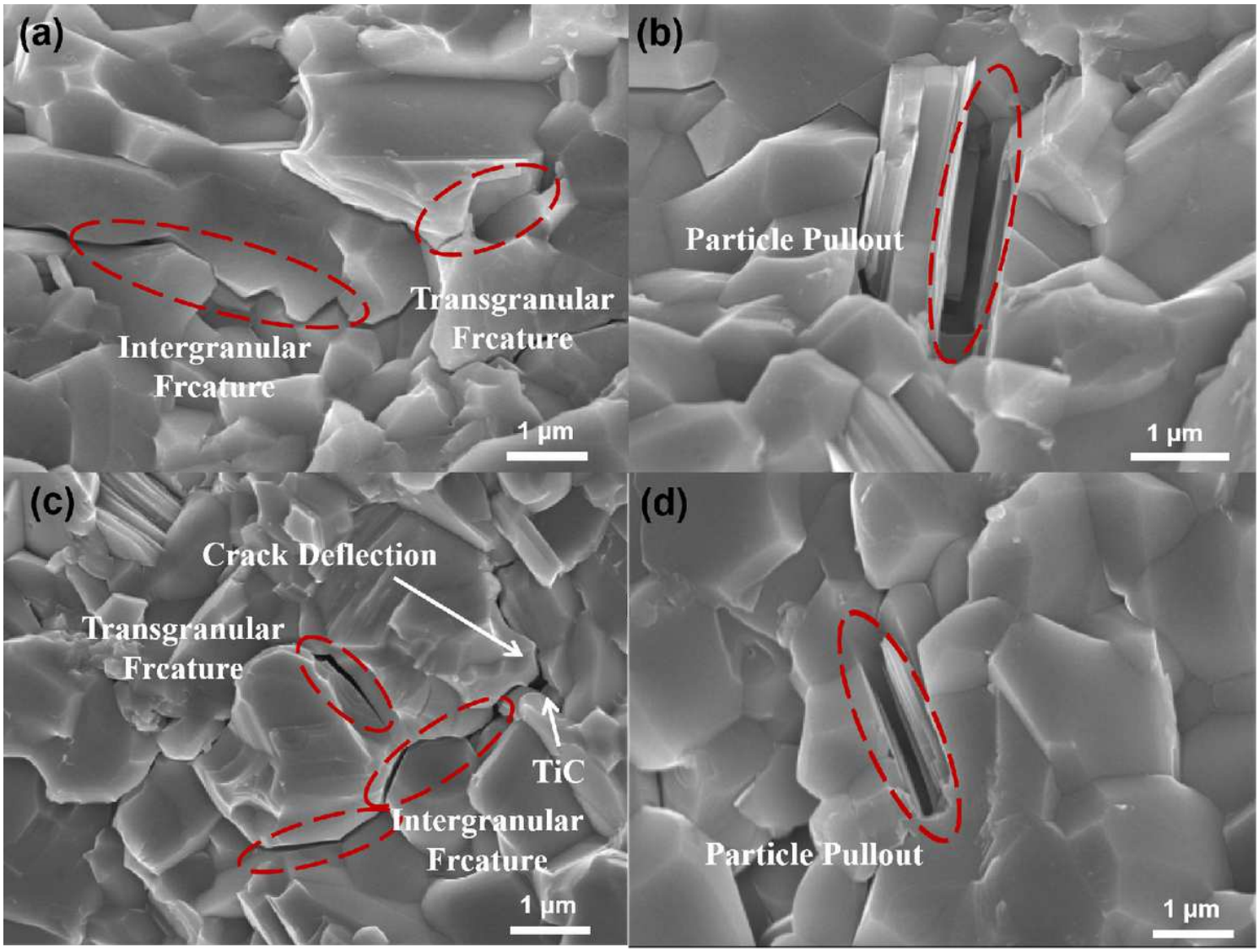

Figure 6

Fracture mode for sample 4:(a) and (b); sample 5: (c) and (d).

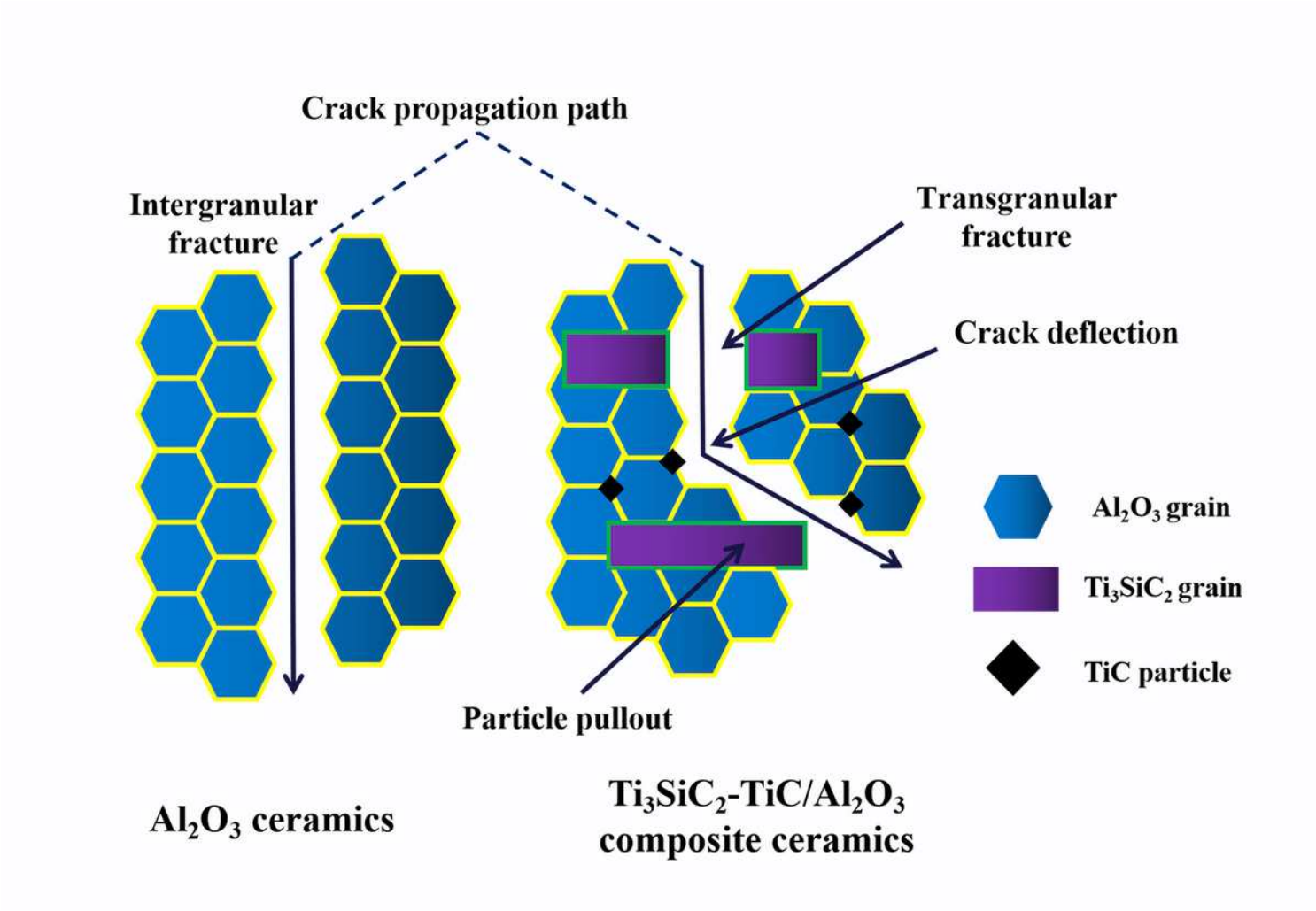

Figure 7

The diagram of microcrack propagation paths in Al2O3 and Ti3SiC2-TiC/Al2O3 ceramics.